

## Attitude Control of a Tilt-rotor Tailsitter Micro Air Vehicle Using Incremental Control

Lovell-Prescod, Gervase H.L.H.; Ma, Ziqing; Smeur, Ewoud J.J.

**DOI**

[10.1109/ICUAS57906.2023.10156272](https://doi.org/10.1109/ICUAS57906.2023.10156272)

**Publication date**

2023

**Document Version**

Final published version

**Published in**

2023 International Conference on Unmanned Aircraft Systems, ICUAS 2023

**Citation (APA)**

Lovell-Prescod, G. H. L. H., Ma, Z., & Smeur, E. J. J. (2023). Attitude Control of a Tilt-rotor Tailsitter Micro Air Vehicle Using Incremental Control. In *2023 International Conference on Unmanned Aircraft Systems, ICUAS 2023* (pp. 842-849). (2023 International Conference on Unmanned Aircraft Systems, ICUAS 2023). IEEE. <https://doi.org/10.1109/ICUAS57906.2023.10156272>

**Important note**

To cite this publication, please use the final published version (if applicable).  
Please check the document version above.

**Copyright**

Other than for strictly personal use, it is not permitted to download, forward or distribute the text or part of it, without the consent of the author(s) and/or copyright holder(s), unless the work is under an open content license such as Creative Commons.

**Takedown policy**

Please contact us and provide details if you believe this document breaches copyrights.  
We will remove access to the work immediately and investigate your claim.

***Green Open Access added to TU Delft Institutional Repository***

***'You share, we take care!' - Taverne project***

**<https://www.openaccess.nl/en/you-share-we-take-care>**

Otherwise as indicated in the copyright section: the publisher is the copyright holder of this work and the author uses the Dutch legislation to make this work public.

# Attitude Control of a Tilt-rotor Tailsitter Micro Air Vehicle Using Incremental Control

1<sup>st</sup> Gervase H.L.H. Lovell-Prescod

Department of Control and Operations

Delft University of Technology

Delft, The Netherlands

G.H.L.H.Lovell-Prescod@student.tudelft.nl

2<sup>nd</sup> Ziqing Ma

Department of Control and Operations

Delft University of Technology

Delft, The Netherlands

Z.Ma@tudelft.nl

3<sup>rd</sup> Ewoud J.J. Smeur

Department of Control and Operations

Delft University of Technology

Delft, The Netherlands

E.J.J.Smeur@tudelft.nl

**Abstract**—Tailsitter Micro Air Vehicles with two rotors are promising due to their simplicity and efficient forward flight, but actuator saturation due to ineffective pitch control at a high angle of attack flight is a challenge limiting the flight envelope. This paper proposes a novel tilt-rotor tailsitter design which features two tilting rotors as the only means for control moment generation. Incremental Nonlinear Dynamic Inversion (INDI) is applied to the attitude control problem of the tilt-rotor tailsitter, whose attitude angle tracking performance is validated by indoor and outdoor flight tests. It is found that actuator saturation is largely avoided by using thrust vectoring which provides sufficient capability of pitch moment generation. However, it is also found that the proposed design with only leading-edge tilting motors excluding any aerodynamic control surfaces has limited roll control effectiveness in forward flight.

**Index Terms**—Tailsitter, Incremental control, Thrust vectoring, Actuator saturation

## I. INTRODUCTION

Over the last few decades Micro Air Vehicles (MAVs) have experienced tremendous development. MAVs are increasingly being used for various applications, ranging from the inspection of infrastructure and the monitoring of crops to reconnaissance and surveillance missions [1]. Some of these missions require MAVs to be capable of hovering as well as fast-forward flight and the rapid transition between the two, which brings about the high demand for hybrid MAVs that combine the advantages of both fixed-wing aircraft and rotorcrafts. Among different kinds of hybrid MAVs, tailsitters are special for their way of transitioning between hovering and forward flight by pitching either up or down 90°, which allows them to use the same actuators in hover as well as forward flight.

Despite the rapid and promising development, traditional tailsitters are faced with the challenge of actuator saturation, which has been mentioned or alluded to in [2], [3] and [4]. During the forward flight, in addition to 'prop-wash' airflow from the leading-edge mounted motors, there is sufficient velocity-induced airflow over the flaps. However, in vertical flight, the velocity-induced airflow is nonexistent in the hovering case, low in the slow climb case and negative in the descent case, which degrades the flap control effectiveness

compared to the forward flight phase. In [5], Ma et al. discovered from the wind tunnel tests of a wing that the flap control effectiveness is much lower at high angles of attack than around zero angles of attack, demonstrating that the flap control effectiveness is limited during the transition and the vertical descent. Consequently, the limited flap control effectiveness leads to potential actuator saturation. Therefore, Bronz [6] compared pitch moment generation with a trailing edge aerodynamic surface on a wing, compared to thrust vectoring with a rotor in front of the wing. For the configuration tested, the pitching moment generated through thrust vectoring was almost twice that produced by the same deflection of flaps. Inspired by using thrust vectoring for control moment generation, a novel configured tailsitter is proposed in this paper, namely a tilt-rotor tailsitter.

Given a novel-designed tilt-rotor tailsitter, it is important to achieve stable control of it. The flight control of tailsitters is a well-studied subject. The high non-linearity of tailsitters makes accurate modeling difficult and resource-intensive. To avoid resource-intensive modeling, Incremental Nonlinear Dynamic Inversion (INDI) control, as a sensor-based technique, has been widely applied by researchers on tailsitters. Smeur et al. [2] applied INDI control to both attitude and velocity control of a tailsitter for the entire flight envelope, demonstrating that all that is required for the robust control of a tailsitter is an expression for the effectiveness of the actuators on the control degrees of freedom. This expression for effectiveness was acquired through flight tests. Yang et al. [3] and Tal et al. [7] also implemented INDI control for the control of tailsitters. The former incorporated a mathematical model of the effectiveness of the actuators and the latter made use of a simplified  $\phi$ -theory aerodynamic forces and moments model to derive expressions for control inputs and states in terms of flat outputs allowing for fully nonlinear inversion. Due to low dependency on modeling, an INDI control law is also derived and implemented for the attitude control of the novel-designed tilt-rotor tailsitter.

The contribution of this paper is the attitude control of a newly designed and built tilt-rotor tailsitter with the INDI control strategy and the validation of the control performance by flight tests, which also demonstrates alleviation of actuator

Corresponding author: Z.Ma@tudelft.nl

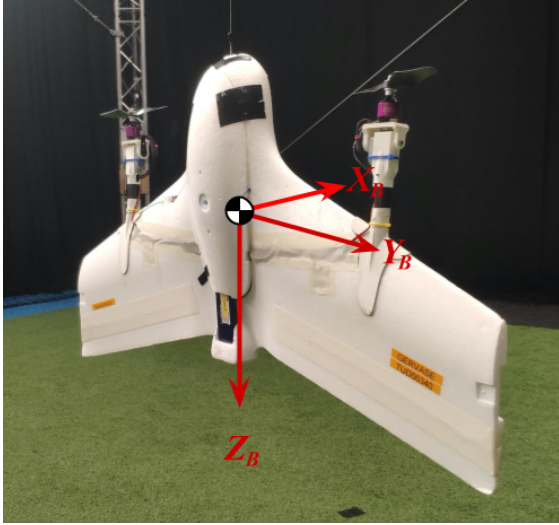


Fig. 1. Body axis system of the tilt-rotor tailsitter.

saturation with the use of thrust vectoring. However, it is also found in this research that the proposed tilt-tailsitter with only leading-edge mounted motors for control moment generation has the drawback of unreliable roll control performance during the forward flight. This paper is structured as follows. Firstly, the physical design of a tilt-rotor tailsitter is outlined in section II. The derivation and adaption of the INDI control law for the presented tilt-rotor tailsitter is described in section III along with the actuator dynamics and other considerations necessary for the successful implementation. Both indoor and outdoor flight test results are displayed in section IV, followed by the discussion on actuator saturation for the tilt-rotor tailsitter in section V. Lastly, conclusions are drawn in section VI together with the prospective future work.

## II. VEHICLE DESIGN

### A. Platform Configuration

Fig. 1 shows a picture of the designed and built tilt-rotor tailsitter. Similar to the traditional tailsitters presented in [8], [2], [3], [7], [4], [9], this proposed tilt-rotor tailsitter has two motors mounted on its wing's leading edge. Instead of having aerodynamic control surfaces, the vehicle is equipped with servos to tilt the two motors individually. Fig. 1 defines the body axis system for the tilt-rotor tailsitter, with the Euler angles  $\phi$ ,  $\theta$  and  $\psi$  defined with respect to the hovering condition shown in the figure. The ZXY Euler rotation sequence is adopted throughout this paper to avoid singularities at  $\pm 90^\circ$  pitch [2]. The left and right thrust in Newton are denoted  $T_l$  and  $T_r$ , respectively, and the left and right tilt angles in radians are denoted  $\delta_l$  and  $\delta_r$ , respectively. With these four actuators, four Degrees of Freedom (DOFs) can be controlled.

### B. Physical specifications

The airframe of the tilt-rotor tailsitter is the off-the-shelf Skywalker x5 Expanded Polyolefin (EPO) foam airframe, into which a carbon fiber spar was added for stiffness.

TABLE I  
INVENTORY OF BUILD COMPONENTS

Component	Name	Qty.
Autopilot	mRo Pixracer R15	1
Motor	Hacker motors A20-20L EVO kV1022	2
ESC	T-motor F35A 3-6s	2
Servo	MKS HV9767	2
GPS	GPS NEO-M8N BDS Compass	1
Battery	Turnigy 3300mAh 4S 25C LiPo	1

The motors and servos are mounted with 3D printed parts. The tilt-rotor tailsitter MAV has a weight of 1.27kg and a wingspan of 1.0m. Each motor has a lateral distance to the center of gravity of 0.3m, denoted by  $b$  in Fig. 2. Longitudinally, the distance between the axis of each tilt servo to the center of gravity is 0.135m, denoted by  $l$ . Moreover, the maximum deflection angle of the tilt servos is  $55^\circ$ , and an inventory of the main electronic components used for the drone is presented in Table I.

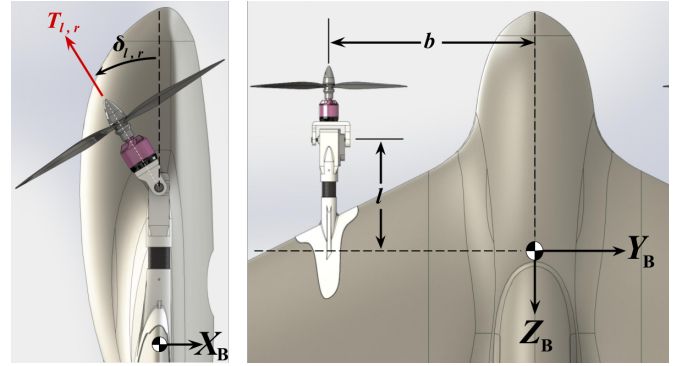


Fig. 2. Definition of the positive deflection angles of the left & right motors  $\delta_l$  &  $\delta_r$ , respectively as well as the scalar distances of each motor from the CG.

## III. ATTITUDE CONTROL

### A. Incremental Nonlinear Dynamic Inversion

INDI control is a sensor-based control technique resting on the notion that both internal and external forces and moments acting on a rigid body (such as due to wind disturbances) will cause linear and angular accelerations which can be derived from accelerometer and gyroscope measurements. We denote the angular velocity vector of the vehicle by  $\Omega$ , the velocity vector in the body frame by  $v$ , the tilt angle of servos by  $\delta$  and the angular velocity of the left and right rotors by  $\omega = [\omega_l \ \omega_r]^T$ . In this paper, it is assumed that the inertia change due to the tilt rotors is small and can be neglected. Taking a diagonal inertia matrix  $I$ , Euler's equation for rotational motion is given by:

$$I\dot{\Omega} + \Omega \times I\Omega = M_c(\omega, \delta) + M_a(\Omega, v), \quad (1)$$

where the total moment is written as the sum of the moment due to aerodynamic effects  $M_a$  and the moment due to control inputs  $M_c$ . The control moment  $M_c$  is a function of

the angular rates of the motors and the tilt angle of the left and right servos, and is given by the following equation:

$$\mathbf{M}_c = \begin{bmatrix} L \\ M \\ N \end{bmatrix} = \begin{bmatrix} -T_r b \cos \delta_r + T_l b \cos \delta_l \\ T_r l \sin \delta_r + T_l l \sin \delta_l \\ T_r b \sin \delta_r - T_l b \sin \delta_l \end{bmatrix}, \quad (2)$$

where  $\mathbf{L}$ ,  $\mathbf{M}$  and  $\mathbf{N}$  refer to the control moments around  $X_B$ ,  $Y_B$  &  $Z_B$  axes respectively. As is defined in Figure 2,  $T_l$  and  $T_r$  are functions of the angular velocity  $\omega$  of each motors and  $\delta_l$  and  $\delta_r$  are tilt angles of the left and right servos.

Equation 1 can be inverted to obtain an expression for the angular acceleration  $\dot{\Omega}$ :

$$\dot{\Omega} = \mathbf{I}^{-1} (\mathbf{M}_a(\Omega, \mathbf{v}) - \Omega \times \mathbf{I}\Omega) + \mathbf{I}^{-1} \mathbf{M}_c(\omega, \delta). \quad (3)$$

We assume that the drone will rotate relatively slowly, such that the term  $\Omega \times \mathbf{I}\Omega$  can be neglected compared to the other terms. We can then apply a first-order Taylor expansion:

$$\begin{aligned} \dot{\Omega} = & \dot{\Omega}_0 + \frac{\partial}{\partial \Omega} (\mathbf{I}^{-1} \mathbf{M}_a(\Omega, \mathbf{v}_0)) \Big|_{\Omega=\Omega_0} (\Omega - \Omega_0) \\ & + \frac{\partial}{\partial \mathbf{v}} (\mathbf{I}^{-1} \mathbf{M}_a(\Omega_0, \mathbf{v})) \Big|_{\mathbf{v}=\mathbf{v}_0} (\mathbf{v} - \mathbf{v}_0) \\ & + \frac{\partial}{\partial \omega} (\mathbf{I}^{-1} \mathbf{M}_c(\omega, \delta_0)) \Big|_{\omega=\omega_0} (\omega - \omega_0) \\ & + \frac{\partial}{\partial \delta} (\mathbf{I}^{-1} \mathbf{M}_c(\omega_0, \delta)) \Big|_{\delta=\delta_0} (\delta - \delta_0). \end{aligned} \quad (4)$$

As was proven in [10], the terms not related to the actuators can be neglected if very fast actuator dynamics are assumed. Therefore, it is assumed that the partial derivatives w.r.t.  $\Omega$  and  $\mathbf{v}$  have a far smaller effect than the partial derivatives w.r.t.  $\omega$  and  $\delta$ , and as such the neglecting of the partial derivatives of  $\mathbf{M}_a$  w.r.t. both the angular velocity  $\Omega$  and the linear velocity  $\mathbf{v}$  is justified. We further consider the specific force in the negative  $Z_B$ -axis,  $T_Z$ :

$$T_Z = \frac{1}{m} (T_l \cos \delta_l + T_r \cos \delta_r), \quad (5)$$

where  $m$  is the mass of the MAV.

A desired thrust in the  $Z_B$ -axis should be fulfilled with the two motors which also have control authority over the other control DOFs, meaning that the desired thrust increment must be allocated keeping into consideration the other control DOFs. Also applying a Taylor expansion to this equation and combining it with Equation 4 yields:

$$\begin{bmatrix} \dot{\Omega} \\ T_Z \end{bmatrix} = \begin{bmatrix} \dot{\Omega}_0 \\ T_{Z_0} \end{bmatrix} + \mathbf{G}(\mathbf{u} - \mathbf{u}_0), \quad (6)$$

where the control input vector  $\mathbf{u}$  is defined as follows:

$$\mathbf{u} = [\delta_l \quad \delta_r \quad \omega_r \quad \omega_l]^\top, \quad (7)$$

and with the control effectiveness matrix  $\mathbf{G}$  defined analytically as:

$$\mathbf{G} = \begin{bmatrix} \mathbf{I}_{\{3 \times 3\}}^{-1} & 0 \\ 0 & \frac{1}{m} \end{bmatrix} \cdot \begin{bmatrix} -b T_l s \delta_l & b T_r s \delta_r & -b \frac{\partial}{\partial \omega_r} (T_r) c \delta_r & b \frac{\partial}{\partial \omega_l} (T_l) c \delta_l \\ l T_l c \delta_l & l T_r c \delta_r & l \frac{\partial}{\partial \omega_r} (T_r) s \delta_r & l \frac{\partial}{\partial \omega_l} (T_l) s \delta_l \\ -b T_l c \delta_r & b T_r c \delta_r & b \frac{\partial}{\partial \omega_r} (T_r) s \delta_r & -b \frac{\partial}{\partial \omega_l} (T_l) s \delta_l \\ T_l s \delta_l & T_r s \delta_r & \frac{\partial}{\partial \omega_r} (T_r) c \delta_r & \frac{\partial}{\partial \omega_l} (T_l) c \delta_l \end{bmatrix}, \quad (8)$$

where ‘s’ and ‘c’ represent sine and cosine operations.

Equation 6 can be inverted to obtain the INDI control law given by:

$$\mathbf{u}_c = \mathbf{u}_f + \mathbf{G}^+ \left( \boldsymbol{\nu} - \begin{bmatrix} \dot{\Omega}_f \\ T_{Z_f} \end{bmatrix} \right), \quad (9)$$

where  $\mathbf{u}_c$  is the new commanded input,  $\boldsymbol{\nu}$  is the virtual control and the superscript ‘+’ represents the Moore-Penrose pseudo-inverse. To remove noise from measured signals, all signals with subscript 0 are filtered with the same filter in order to keep these signals synchronized [11], indicated with the subscript  $f$ . Since the angular acceleration  $\dot{\Omega}_f$  in Equation 9 is from measurements, the impact of wind disturbances can be compensated through the control increments. A summary of the control law in the form of a block diagram is presented in Fig. 3.

The angular rates can be controlled with simple proportional feedback as is shown in Equation 10 below.

$$\boldsymbol{\nu} = K_\Omega (\Omega_{\text{ref}} - \Omega). \quad (10)$$

The attitude can be controlled by a second proportional feedback controller using the feedback of the vector part of the quaternion error [12]:

$$\Omega_{\text{ref}} = K_\eta \begin{bmatrix} q_{\text{err}1} \\ q_{\text{err}2} \\ q_{\text{err}3} \end{bmatrix}, \quad (11)$$

where the vector of quaternion errors  $\mathbf{q}_{\text{err}}$  represents the error between the reference attitude in quaternion form  $\mathbf{q}_{\text{ref}}$  and the state quaternion  $\mathbf{q}_s$ , as is given by the following equation:

$$\mathbf{q}_{\text{err}} = \mathbf{q}_{\text{ref}} \otimes \mathbf{q}_s^*, \quad (12)$$

where ‘ $\otimes$ ’ is the Kronecker product and the superscript ‘\*’ represents the conjugate.

## B. Actuator Dynamics

The INDI control law relies heavily on the relationship between control inputs and measured outputs, meaning knowledge of the actuator states is important. As actuator state feedback is not available in this case, we employ a model of the actuator to estimate its state. A servo dynamics experiment was conducted to identify the dynamics of the tilt mechanism, using a gyroscope mounted to the servo arm as shown in Fig. 4.

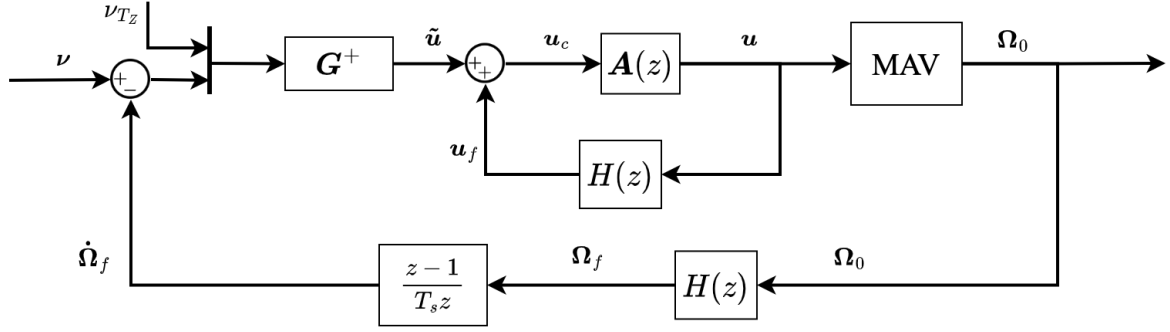


Fig. 3. Block diagram of the derived control law and its relation to the MAV



Fig. 4. Experimental setup of servo dynamics experiment

The tilt dynamics of the servos are described by a second-order transfer function as follows:

$$A(s) = e^{-\tau_d s} \cdot \frac{\omega_n^2}{s^2 + 2\zeta\omega_n s + \omega_n^2}, \quad (13)$$

where  $\tau_d$  is the actuator delay,  $\omega_n$  is the actuator natural frequency and  $\zeta$  is the damping ratio. This response is then passed through a rate limiter with a rate limit corresponding to the maximum observed angular rate during the experiments. The tilt dynamics are characterized in Table II. The equivalent discrete transfer function is given by the following equation at a sampling frequency of 500 Hz:

$$A(z) = z^{-7} \cdot \frac{0.01175z^{-1} + 0.01079z^{-2}}{1 - 1.752z^{-1} + 0.7741z^{-2}} \quad (14)$$

TABLE II  
SUMMARY OF ACTUATOR DYNAMICS CHARACTERISTICS

Tilt servo delay, $\tau_d$	14	[ms]
Tilt servo natural frequency, $\omega_n$	76	[rad/s]
Tilt servo damping ratio, $\zeta$	0.8	[-]
Tilt servo rate limit	11.34	[rad/s]

The linear mapping relationship between the servo Pulse Width Modulation (PWM) command  $c_\delta$  and the angle in degrees is obtained and given by:

$$\delta_{l,r} = 0.1096 \cdot c_\delta, \quad (15)$$

Moreover, to express the thrust as a function of the angular rate  $\omega_{l,r}$ , static thrust tests using the RCBenchmark 1580

motor test bench were conducted<sup>1</sup>. The following thrust expression in Newton is obtained for the motor-ESC pair outlined in subsection II-B.

$$T_{l,r}(\omega_{l,r}) = 5.0 \cdot 10^{-6} \omega_{l,r}^2 - 8.0 \cdot 10^{-4} \omega_{l,r} + 0.10 \quad (16)$$

where angular rate  $\omega_{l,r}$  as a function of motor PWM command  $c_T$  is given by:

$$\omega(c_T) = -6.0 \cdot 10^{-4} c_T^2 + 3.1 c_T - 2.6 \cdot 10^3. \quad (17)$$

### C. Implementation

The attitude control law derived in subsection III-A was applied alongside the actuator dynamics modeled in subsection III-B within the Paparazzi open-source autopilot software[13]. The following three sections highlight aspects taken into consideration for the successful implementation of the INDI control law on the presented tilt-rotor tailsitter.

1) *Filtering*: Given the fact that the angular accelerations are obtained through the differentiation of the measured angular rates from the onboard gyroscope, the measured rates will be inevitably noisy due to the presence of vibrations in the airframe and the noise inherent to the gyroscope. Therefore, the gyroscope measurements are filtered with a second-order Butterworth filter, whose transfer function in the Laplace domain is given by:

$$H(s) = \frac{\omega_c}{s^2 + 2\zeta\omega_c s + \omega_c^2}, \quad (18)$$

with the corner frequency  $\omega_c$  of 6.28 rad/s (1 Hz) and damping ratio  $\zeta$  of 0.707. The equivalent discrete transfer function of the applied filter  $H(z)$  was then obtained through the Tustin transform at 500 Hz.

Furthermore, as the axis around which the tilting mechanism rotates is parallel to the  $Y_B$ -axis, additional noise is observed for the pitch rate measurements. This noise then propagates through the control loop via the calculation of the angular acceleration setpoint. A first order low-pass filter with corner frequency  $\omega_c$  of 12.56 rad/s (2 Hz) is introduced in the feedback of the body rates for the  $Y_B$ -axis. Equation 10 can be updated accordingly and is given as follows:

<sup>1</sup><https://www.tytorobotics.com/pages/series-1580-1585>

$$\nu = K_{\Omega} \left( \Omega_{\text{ref}} - \begin{bmatrix} p \\ q_{fLP} \\ r \end{bmatrix} \right) \quad (19)$$

Where the subscript ‘ $f_{LP}$ ’ indicates the low-pass filtered signal.

2) *Control Allocation Priorities*: To avoid exceeding the actuator limits with Equation 9, the Weighted Least Squares (WLS) control allocation algorithm was employed in order to give priorities to the control objectives [14]. In this implementation the relative priority factors fed to the WLS control allocation algorithm are [1, 1, 1, 10] for rotations around the  $X_B$ -,  $Y_B$ -,  $Z_B$ -axes and thrust in the negative  $Z_B$ -axis direction respectively.

Additionally, if the motor throttle level is reduced to 0%, the control effectiveness of the associated tilt becomes 0, making the matrix  $G$  singular and creating an impossibility for the control allocation algorithm. To prevent this, a minimum throttle level is required for each motor, respectively 41.6% for vertical flight and 21% for horizontal flight. Note that the nominal throttle setting for hovering is approximately 70%, leaving sufficient range for differential thrust.

3) *Constraining Control Objective*: The INDI control law and WLS control allocation rely on the linearization of the control forces in Equation 4, which can lead to linearization errors if the commanded control input is far away from the linearization point. We propose to constrain the control increment to the vicinity of the linearization point in this paper. On the one hand, the maximum setpoint for roll, pitch and yaw rates is set as  $\pm 2$  rad/s (approx. 115 deg/s). On the other hand, a maximum increment of 25 deg is set for each tilt, which is determined by the comparison between the angular acceleration computed with the linearized control effectiveness in Equation 8 and that computed with the nonlinear equations for the control moments in Equation 2. It was found that a tilt increment of approximately 25 deg resulted in an error of 3.3%.

#### IV. FLIGHT TEST RESULTS

To evaluate the performance of thrust vectoring as the only means of control moment generation, both indoor and outdoor tests have been conducted. The results of the performed flight tests are demonstrated in the following section.

##### A. Indoor Flight Test

Multiple indoor flight tests were conducted in a  $10m \times 10m$  flight arena, in order to verify the implemented INDI attitude control law and the modeled actuator dynamics. Due to the limited space, only hovering tests were performed indoors.

Fig. 5 presents the comparison between references and measurements for Euler angles, and for angular jerk responses as well. The reason for evaluating angular jerk responses is that the control effectiveness matrix  $G$  maps increments in control inputs to angular jerk responses directly. Specifically, the references and measurements are respectively calculated and measured roll, pitch and yaw angles and angular jerk responses to the same actuator input

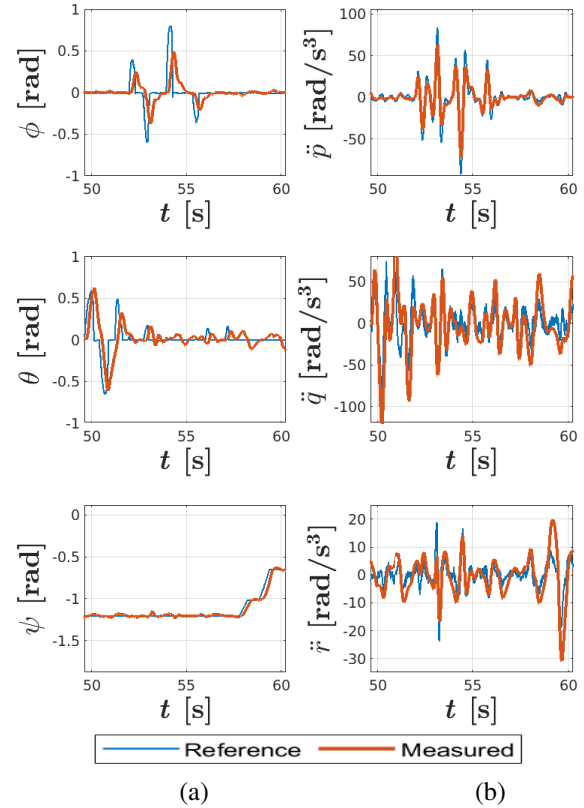


Fig. 5. (a) Reference versus measured Euler angles for the indoor vertical flight test; (b) Reference versus measured angular jerks for the indoor vertical flight test.

from one indoor vertical flight test. The figure shows that the measured Euler angles are able to keep a generally good track of the reference attitude angles. It can also be seen from the figure that the measured angular jerk responses mostly align with the angular jerks calculated from the control derivatives, verifying that the actuator dynamics and actuator control effectiveness have been accurately modeled. Nevertheless, some discrepancies in magnitude are also observed which can be explained by the difference between the actual thrust and the computed thrust according to the static test results. Though not considering wind disturbances, the indoor flight test results validate the successful implementation of the INDI attitude control law for the tilt-prop tailsitter during vertical flight.

##### B. Outdoor flight test

To test the flight performance of the tilt-rotor tailsitter in the whole flight envelope, multiple outdoor flights were conducted. The flight test results presented below were from an approximately six-minute continuous outdoor flight, including hovering and forward flight and transitions between the two.

Fig. 6 depicts the tracking performance of the INDI attitude controller for the tilt-rotor tailsitter within the whole envelope, in which gray shaded areas correspond to the forward

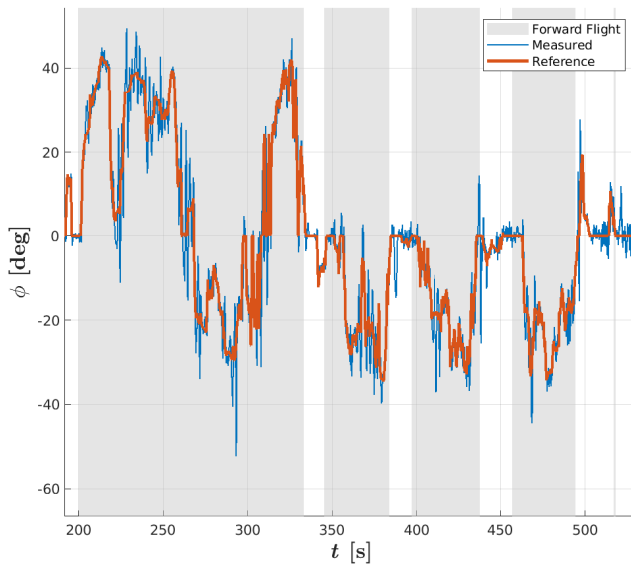
flight phase. It can be observed that during the six-minute flight, eight transitions between hovering and forward flights were performed.

In Fig. 6(a), Fig. 6(b) and Fig. 6(c), the tracking performance for  $\phi$ ,  $\theta$  and  $\psi$  are displayed respectively. It can be seen that the measured attitude angles follow the reference angles accordingly, showing that it is possible to control the vehicle with the approach presented. Nevertheless, in multiple outdoor flight tests, the drawback of the proposed tilt-rotor tailsitter design is also exposed. Fig. 7 presents the roll angle tracking performance and the corresponding actuator states for a 130-second flight that covers the whole flight envelope. During forward flight, notable tracking errors

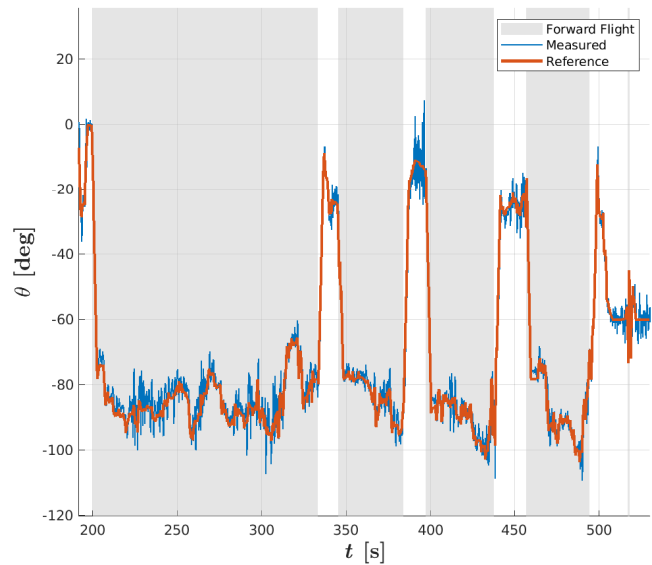
for the roll angle are observed, where the left and right servos have already generated large tilt deflections, showing the deficiency of the tilt-rotor tailsitter with only leading-edge mounted motors for control moment generation.

## V. DISCUSSION

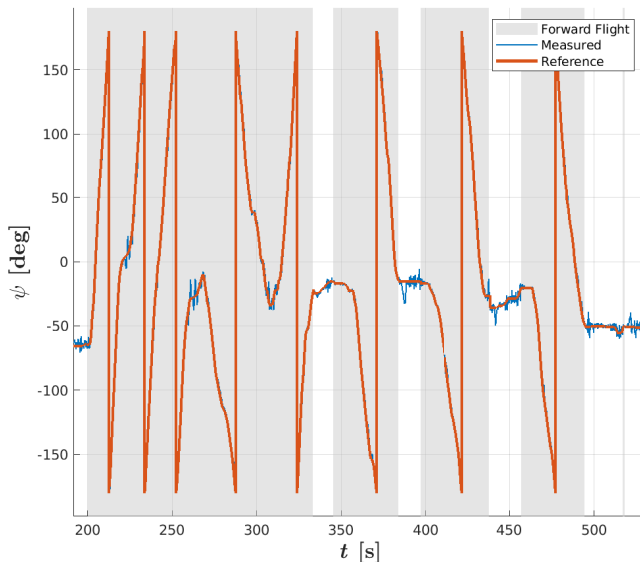
To give an insight into actuator saturation, the actuator states are displayed in Fig. 6(d), in which the motor states are shown as a percentage of their maximum throttle setting and servo states directly as tilt angles in degrees. Even if the tilt angle command exceeds the lower limit at very rare moments (around 265s and 310s) due to overshoot, throughout the entire flight, the incremental control inputs for tilt angles are



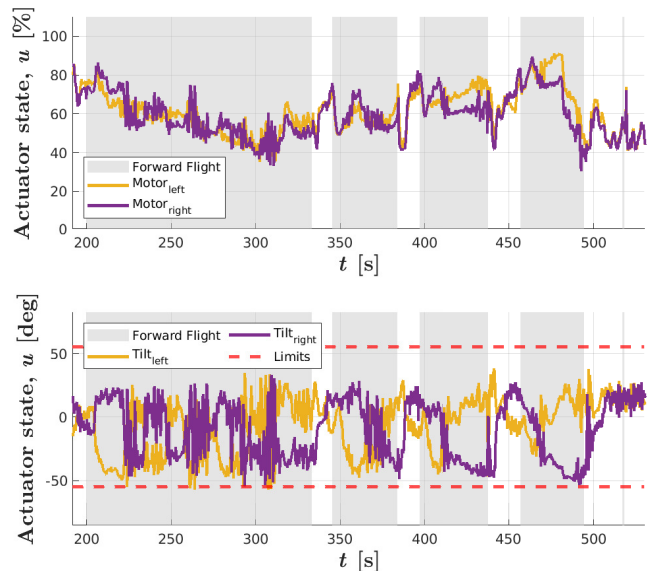
(a) Roll  $\phi$  measured and reference angles for the flight (ZXY Euler)



(b) Pitch  $\theta$  measured and reference angles for the flight (ZXY Euler)

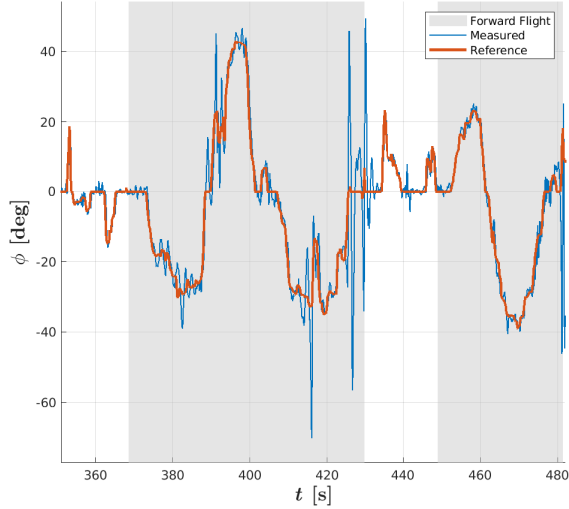


(c) Yaw  $\psi$  measured and reference angles for the flight (ZXY Euler)

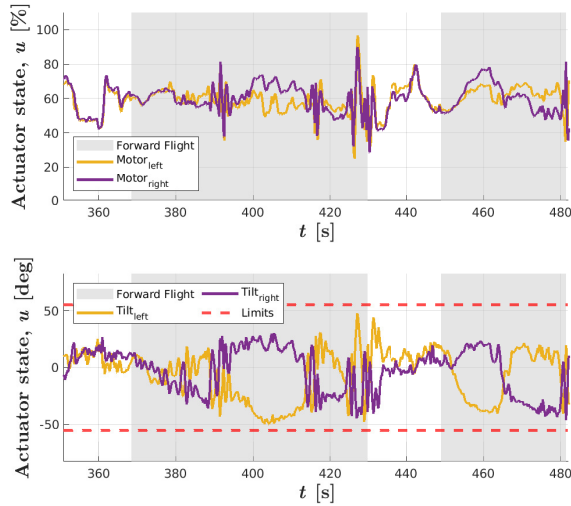


(d) Evolution of actuator states  $u$ , respectively, motor evolution as a percentage of max throttle setting and tilt angle  $\delta_{l,r}$  in degrees.

Fig. 6. Tracking performance of attitude controller for a six-minute flight within the whole envelope, grey shaded areas of all plots represent the horizontal flight phase.



(a) Roll  $\phi$  measured and reference angles for the flight (ZXY Euler)

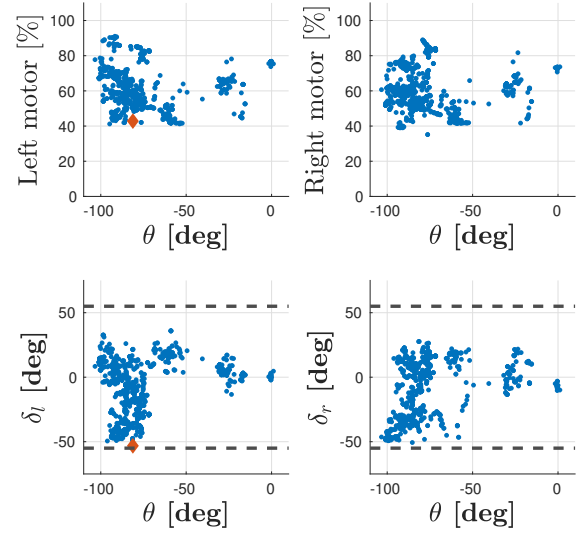


(b) Evolution of actuator states  $u$ , respectively, motor evolution as a percentage of max throttle setting and tilt angle  $\delta_{l,r}$  in degrees.

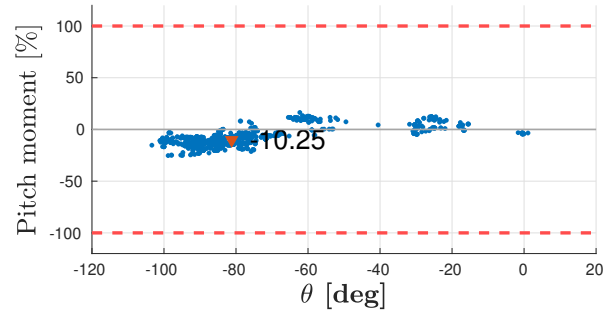
Fig. 7. Tracking performance of controller for a 130-second flight, and grey shaded areas correspond to the forward flight phase

within the range of  $-55^\circ$  to  $55^\circ$ . It is noteworthy that during the entire outdoor test, actuator saturation happens to the left tilt servo  $\delta_l$  three times, with a total time of 0.544s taking up approximately 0.15% of the whole six-minute test.

Fig. 8(a) presents the actuator states at various pitch angles where the vehicle is in pitch equilibrium: the pitch angular acceleration  $\dot{q}$  is very low, specifically,  $-0.5 \leq \dot{q} \leq 0.5$  [deg/s<sup>2</sup>] and  $-5 \leq q \leq 5$  [deg/s]. The red diamond in the figure refers to an instance of left tilt saturation of  $-55$  deg. However, the corresponding left motor throttle is only 43% and the percentage of pitch moment to the maximum pitch moment generation availability is -10.25% as is shown in Fig. 8(b). Despite the instance of the left tilt, there is still



(a) Tilt deflections  $\delta_{l,r}$  at varying pitch  $\theta$  angle equilibrium points



(b) Pitch control moment as percentage of total available pitch moment generation capability.

Fig. 8. Illustration of pitch moment generation availability despite the occurrence of saturation of left tilt.

sufficient availability for pitch moment generation. It can be concluded that actuator saturation is significantly avoided by the application of thrust vectoring, which provides sufficient pitch moment generation capability even with the occasional occurrence of actuator saturation.

Though saturation does not happen often, it can be seen that the tilts show large deflections during forward flight. This raises questions about the effectiveness of the tilts during forward flight, even though the throttle in some of these cases is not low. A possible cause could be the propeller-wing interaction since the propeller is positioned in front of the wing. It should be considered that even though the tailsitter is meant to fly efficiently during forward flight, flight efficiency may be reduced due to these large deflections.

## VI. CONCLUSION

This paper presents a novel configuration of tilt-rotor tailsitter which exclusively uses thrust vectoring for control moment generation. Different from traditional tailsitters, it features two motors mounted on tilting mechanisms. An

Incremental Nonlinear Dynamic Inversion (INDI) control law is derived and implemented for the attitude control of the proposed vehicle. Outdoor test flights demonstrate attitude angle tracking for the whole flight envelope. Furthermore, it is found that the use of thrust vectoring for control moment generation avoids actuator saturation which only takes up 0.15% of the flight time. However, from the large differential deflections of the motor tilts during forward flight it can be concluded that the roll control is not very effective in this flight phase.

Given the fact that the roll control of the tilt-rotor tailsitter is shown to be poor during forward flight, quantitative and qualitative comparisons for respectively pitch, roll and yaw moment generation between thrust vectoring and flap deflection will be addressed in future work. Overall, this paper demonstrates both the physical feasibility of exclusively using thrust vectoring in tailsitters as well as the adaptation of the INDI control law for the control of such tailsitters.

#### REFERENCES

- [1] A. S. Saeed *et al.*, “A survey of hybrid Unmanned Aerial Vehicles,” *Progress in Aerospace Sciences*, vol. 98, no. December 2017, pp. 91–105, 2018. [Online]. Available: <https://doi.org/10.1016/j.paerosci.2018.03.007>
- [2] E. J. Smeur, M. Bronz, and G. C. de Croon, “Incremental control and guidance of hybrid aircraft applied to a tailsitter unmanned air vehicle,” *Journal of Guidance, Control, and Dynamics*, vol. 43, no. 2, pp. 274–287, 2020.
- [3] Y. Yang *et al.*, “Robust proportional incremental nonlinear dynamic inversion control of a flying-wing tailsitter,” *Proceedings of the Institution of Mechanical Engineers, Part G: Journal of Aerospace Engineering*, vol. 234, no. 16, pp. 2274–2295, 2020.
- [4] J. Zhong *et al.*, “L1 adaptive control of a dual-rotor tail-sitter unmanned aerial vehicle with input constraints during hover flight,” *IEEE Access*, vol. 7, pp. 51 312–51 328, 2019.
- [5] Z. Ma, E. J. Smeur, and G. C. de Croon, “Wind tunnel tests of a wing at all angles of attack,” *International Journal of Micro Air Vehicles*, vol. 14, p. 17568293221110931, 2022.
- [6] M. Bronz, “Comparison of pitching moment generation via flap deflection and thrust vectoring on a generic blown-wing model,” in *AIAA Aviation 2019 Forum*, 2019, p. 3171.
- [7] E. A. Tal and S. Karaman, “Global trajectory-tracking control for a tailsitter flying wing in agile uncoordinated flight,” in *AIAA AVIATION 2021 FORUM*, 2021, p. 3214.
- [8] L. R. Lustosa, F. Defay, and J. M. Moschetta, “Longitudinal study of a tilt-body vehicle: Modeling, control and stability analysis,” *2015 International Conference on Unmanned Aircraft Systems, ICUAS 2015*, pp. 816–824, 2015.
- [9] J. L. Forshaw and V. J. Lappas, “High-fidelity modeling and control of a twin helicopter rotor tailsitter,” *AIAA Guidance, Navigation, and Control Conference 2011*, no. August, pp. 1–16, 2011.
- [10] R. Steffensen, A. Steinert, and E. J. J. Smeur, “Nonlinear dynamic inversion with actuator dynamics: An incremental control perspective,” *Journal of Guidance, Control, and Dynamics*, pp. 1–9, 12 2022. [Online]. Available: <http://arxiv.org/abs/2201.09805https://arc.aiaa.org/doi/10.2514/1.G007079>
- [11] E. J. Smeur, Q. Chu, and G. C. de Croon, “Adaptive incremental nonlinear dynamic inversion for attitude control of micro aerial vehicles,” *2016 AIAA Guidance, Navigation, and Control Conference*, pp. 1–16, 2016.
- [12] E. J. Smeur, G. C. de Croon, and Q. Chu, “Cascaded incremental nonlinear dynamic inversion for MAV disturbance rejection,” *Control Engineering Practice*, vol. 73, no. January, pp. 79–90, 2018. [Online]. Available: <https://doi.org/10.1016/j.conengprac.2018.01.003>
- [13] G. Hattenberger, M. Bronz, and M. Gorraz, “Using the Paparazzi UAV System for Scientific Research,” in *International Micro Air Vehicle Conference and Competition (IMAV)*, 2014, pp. 247–252.
- [14] E. J. Smeur, E. C. Höppener, and D. Wagter, “Prioritized Control Allocation for Quadrotors Subject to Saturation,” *International Micro Air Vehicle Conference and Flight Competition 2017*, pp. 37–43, 2017.